LANGMUIR

pubs.acs.org/Langmuir Article

In Situ Oil Separation and Collection from Water under Surface Wave Condition

Xin Yan, Guohua Liu, Jinliang Xu, and Xiaojing Ma*

Cite This: *Langmuir* 2021, 37, 6257−6267 Read Online

ACCESS | Metrics & More | Article Recommendations | Supporting Information

ABSTRACT: Removal of oil from water is strongly desired due to environmental pollution, and related studies are mainly limited to the material itself. Here, we propose an oil−water separation device, called a floating well, which includes a container for oil collection and a modified mesh screen for oil separation. The mesh screen is superhydrophilic to oil and superhydrophobic to water. The oil removal experiment was performed in a basin. Under the calm surface condition, the oil collection efficiency is shown to be 42−69%. The inadequate oil collection is explained by the breakdown of a thin oil film above water to form an oil-free area, preventing direct contact between the separator and the oil. Sustained by a wave generator, we are surprised to find that with a low-frequency surface wave, the oil collection efficiency is increased to 98%, and the collection speed reaches 2.5 times that under the calm surface condition. The almost complete collection is due to the sustained contact between the separator and the oil, under which the surface wave continuously drives the oil film toward the separator from elsewhere, thus the oil-free area cannot be formed. Our work presents a new clue for large-scale in situ applications, in which the nature wave energy of river/sea can be the driving force for continuous oil separation and collection.

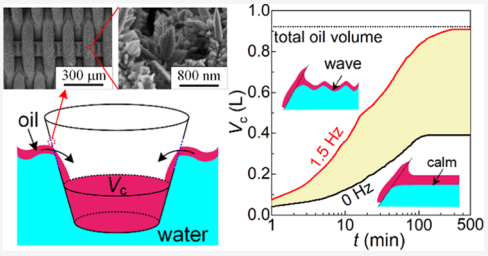

INTRODUCTION

Developments in oil industries come with the expanding oily wastewater and frequent oil-spill accidents, which induce severe water pollution and threatened species in the ecological system.[1] The studies on oil−water separation are thus increasingly important from the environmental, economic, and social points. A variety of oil−water separation techniques have been developed to address the issues.[2−4] Mechanical devices including oil skimmers or booms are used to separate oil/water mixtures, but they require an input of energy or high pressure to operate.[5,6] Porous materials such as sponges, foams, and textiles are also adopted to absorb oil from water.[4,7,8] However, such materials suffer from low capacities/throughput, as they simultaneously absorb both water and oil, resulting in low separation selectivity and efficiency. Moreover, since recycling of these materials is costly, they are generally in situ burned or buried on the ground.[9] This gives rise to secondary pollution of the environment by forming toxic gases and land contamination.

A series of new materials with different affinities toward oil and water have been recently suggested for oil−water separation.[10−14] These materials with special wettability, that can selectively absorb oil (or water) while completely repelling water (or oil), have been successfully applied for oil−water separation on a laboratory scale.[10,11] It is shown that the hydrophilic/oleophobic surface is suitable for separating oil-in-water emulsions, while the hydrophobic/oleophilic surface separates water-in-oil emulsions.[14] The separation process is shown to be energy-efficient and cost-effective, as the mesh separates an oil−water mixture based on different interfacial effects of oil and water on a superwetting surface.[15] Although the hydrophobic/oleophilic materials show high absorption capacity, high selectivity, and good recyclability, these materials are still not applied for practical oil-spill cleanup because of poor volume-based absorption capacity and difficulty in achieving high continuity throughput.[16] For instance, hydrophobic/oleophilic Fe_2O_3/C foams have an amazing mass-absorption capacity of 100; however, the collected oil is only stored in the pores, restricting the volumetric collection capacity.[17,18] Moreover, mechanical handling (squeezing/compressing) is further needed to transport the absorbed oil. This not only disturbs the continuous release of oil from materials but also requires additional energy input.[19,20] Besides, most of the new materials for oil−water separation are only verified on a calm surface in a beaker.[14,21−23] There is a long way to go between them and practical applications.

In this work, we report an in situ oil separation and collection device, called a floating well, for pumpless and continuous recovery of crude oil from a water surface. The floating well includes a container for oil collection and a mesh

Received: March 1, 2021
Revised: April 30, 2021
Published: May 12, 2021

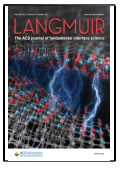

https://doi.org/10.1021/acs.langmuir.1c00585
Langmuir 2021, 37, 6257−6267

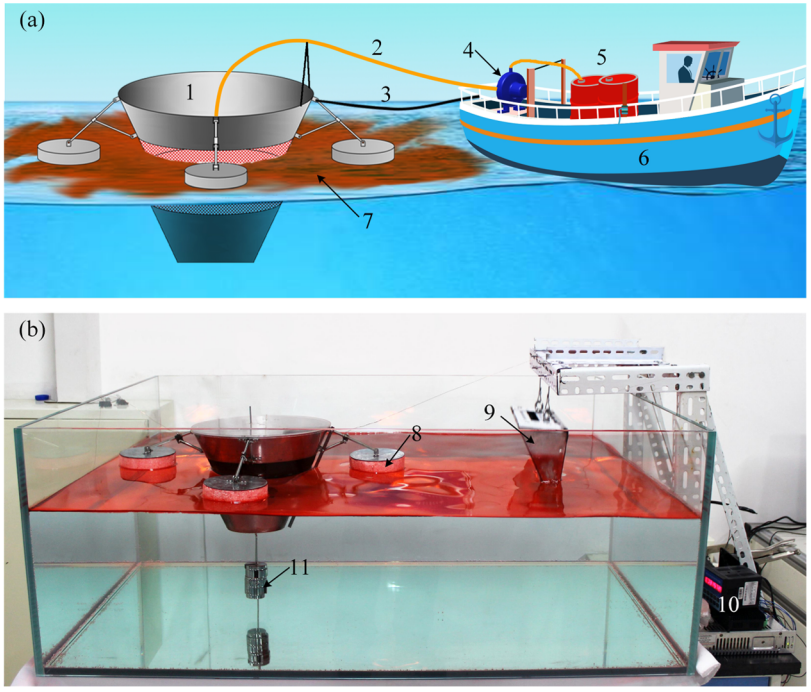

Figure 1. Concept design (a) and real experimental setup (b) of the floating well for oil separation from water (1: floating well, 2: oil tube, 3: rope, 4: oil pump, 5: oil tank, 6: towing ship, 7: oil, 8: buoy, 9: shocking tank, 10: controller, and 11: balance weight).

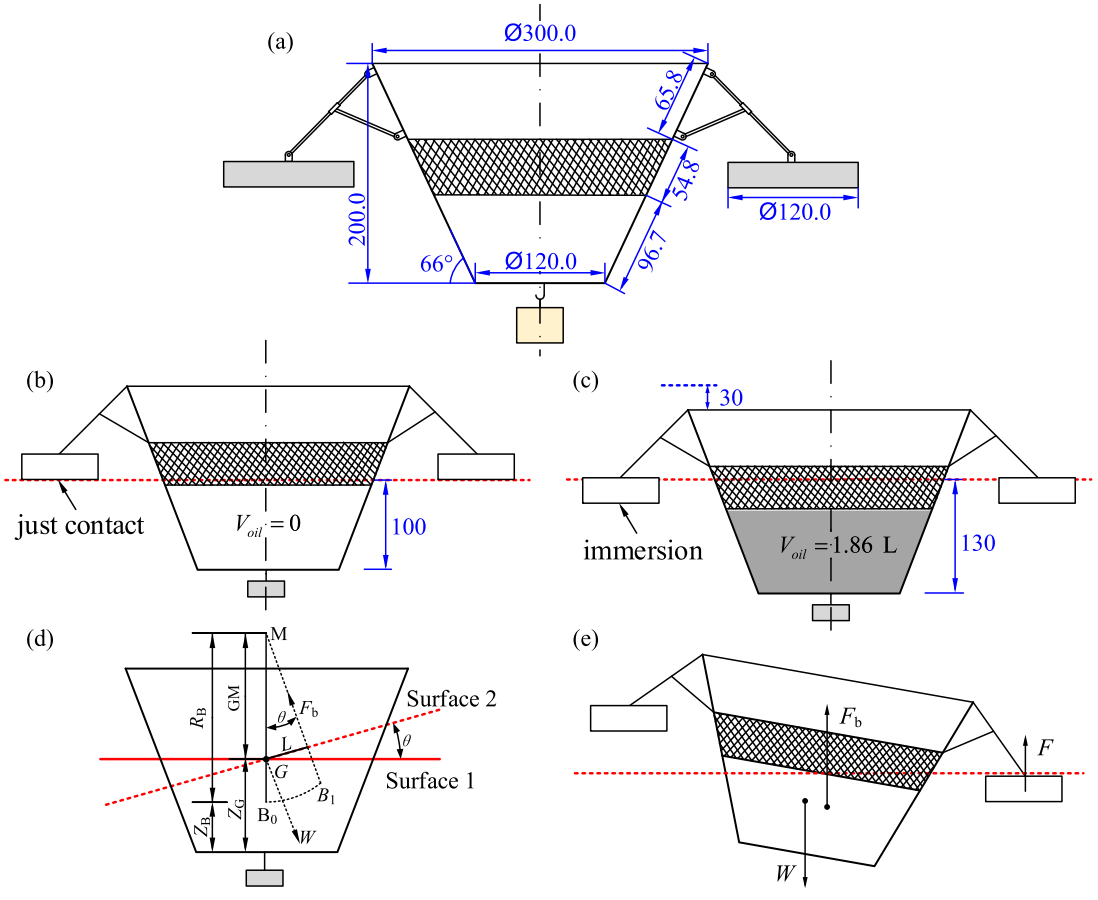

Figure 2. Geometry parameters and stability analysis of the floating well: (a) geometry parameters, (b, c) schematic diagram of the floating well at empty and full load, and (d, e) stability analysis. Note: all units are in millimeters.

screen for oil separation. The mesh screen, fabricated by a facile chemical method, is superhydrophilic to oil and superhydrophobic to water, showing high oil−water separating efficiency. Four auxiliary buoys are applied to enhance the

https://doi.org/10.1021/acs.langmuir.1c00585
Langmuir 2021, 37, 6257−6267

floating-well stability. Due to the integrated functionalities, the floating well allows continuous in situ separation of oil−water mixtures without pumping power. Simultaneous oil filtration and collection are achieved, with high oil−water separation efficiency, leading to a nearly complete oil collection. Flow visualization and force balance analysis confirm that the oil film is driven by wave energy to sustain the oil−water separation process. This wave-driven oil recovery technique is easily scaled for open-sea applications, making it an attractive option for cleanup of large-area oil spills on seawater.

OIL−WATER SEPARATION SYSTEM

Conceptual Design and Demonstration of the Floating Well. An oil−water separation system is designed and scaled up by a floating well, an oil pump, an oil storage tank, a pipeline, and a towing ship (see Figure 1a). The floating well separates the spilled oil from water and in situ stores the collected oil in a barrel. The oil pump transports the stored oil to the oil tank on towing ship. Thus, the device can realize the continuous separation of an oil−water mixture. The floating well is the core equipment of this oil−water separation system. To achieve in situ oil separation and collection, the floating well is composed of a container for oil collection, a modified mesh screen for oil separation, and four buoys to balance the device against waves. The modified mesh screen was integrated on the waist of a conical barrel for better contact with the oil.

Figure 1b presents an image of the verification facility. The size of the water flume is 1800 × 800 × 450 mm^3 with a water level H of 300 mm. The wave generator, composed of a shock tank, a stepping motor, a controller, connecting ropes, and cranks, was used to excite waves simulating the sea wave. The stepping motor drives the shock tank to move up and down, with a tunable stroke (40−100 mm) and a frequency of 0−1.8 Hz. To simulate the spilled oil, a certain volume of liquid paraffin (Aladdin, AR) was poured into the water flume. The liquid paraffin is a colorless mixture obtained from petroleum fractionation. Its main components are alkanes with carbon atom number C9−C13, and the physical properties are shown in Table S1. The liquid paraffin was dyed orange-red with a small amount (0.3 wt %) of Sudan III (Aladdin, AR) to clarify from water, which does not change the paraffin properties.

In the laboratory, the floating well was scaled down to satisfy the water flume (see Figures 1b and 2a). The top and bottom diameters of the barrel are 120 and 300 mm, respectively. The height is 200 mm. The storage capacity of the oil chamber is about 1.86 L. When the oil chamber is empty, the floating well is about 100 mm deep into water (see Figure 2b), while submerges into water with a further 30 mm for full load (see Figure 2c). Four supporting buoys around the floating well play several roles: (1) providing additional buoyancy force to prevent the device from sinking, (2) adjusting the waterline of the device in water, and (3) establishing balance feedback of device to water fluctuation.

Stability Analysis of the Floating Well in a Wave. The mechanical structure and stability of a floating well in a wave are important for practical use. The device stability in ocean current can be analyzed using the stability principle of a ship, in which a restoring moment M_s is produced to restore the device to its equilibrium state.[16] The position of buoyancy center B changes from B_0 to B_1 when the device inclines at a certain angle (see Figure 2d). Thus, the gravity force W and buoyancy force F_b are not in the same line, and an opposite moment $M_s = W{\cdot}GM \sin\theta$ is spontaneously formed to offset the overturning moment, where θ is the dip angle of a self-adaption well. $M_s > 0$ represents the opposite moment formation to avoid the device overturning. Thus, GM should be larger than zero to ensure $M_s > 0$. According to the geometric relationship (see Figure 2d)

$$GM = Z_B + R_B - Z_G \tag{1}$$

where Z_B is the length between the bottom of the device and the buoyancy center B, which can be calculated by $Z_B = \left(1 - \frac{R^2 + 2Rr + 3r^2}{4(R^2 + Rr + 3r^2)}\right){\cdot}h$. Here, R is the radius of the cross section at the waterline, r is the bottom radius of the barrel, and h is the draught. R_B is the radius of the initial stable center and can be calculated as $R_B = I/V_d$. I is the moment of inertia of the cross section at the draught line, which can be obtained by $I = \pi R^4/4$, and V_d is the drainage volume. Z_G is the height of the gravity center, which can be calculated by the weighted mean method of the geometry centers of the device and load. For the floating well without oil load, Z_B, R_B, and Z_G equal to 58, 44, and 32 mm, respectively. When the floating well is fully loaded, 72, 45, and 40 mm are attained for Z_B, R_B, and Z_G, respectively. It is easy to know that GM is always greater than zero no matter an empty or a full load state. Thus, the device has self-adaption stability and can be stable at an inclination angle in the range of 0−15°. It is noted that four supporting buoys are located around the floating well. Once the floating well is inclined, one or more buoys are immersed in water to generate additional buoyancy force to prevent the device from sinking (see Figure 2e).

MATERIALS AND METHODS

Materials. Copper sulfate pentahydrate and stearic acid were purchased from Aladdin Technology Co. Ltd. Ethanol pentahydrate and acetone were purchased from China National Pharmaceutical Group Corporation. All chemicals were used as received without further purification. Deionized water was used in our experiments.

Preparation of Superhydrophobic/Oleophilic Meshes. In this paper, the twill Dutch weaved mesh screen (type 201) was used to prepare a superhydrophobic/oleophilic separator. The mesh screen was initially cleaned in acetone, ethanol, and deionized water using an ultrasonic washing machine. After drying in a vacuum oven with a constant temperature of 60 °C for 30 min, the mesh screen was immersed in a mixture solution of 0.25 M $CuSO_4$ and 0.2 M HCl at room temperature for different time durations (see Figure S1a). The mesh screen was then rinsed with deionized water and dried for 15 min to yield superhydrophilic properties. To obtain a superhydrophobic surface, the copper-coated mesh screen was then soaked in a 0.05 M stearic acid ethanol solution for 30 min (see Figure S1b) followed by drying at 120 °C for 30 min. The wetting ability of the final mesh screen depends on the immersion duration of the two steps. This method is an easily scalable fabrication and can be integrated into an industrial process for high-throughput production.

Characterization. The scanning-electron microscopy (SEM) image of the twill Dutch weaved mesh screen is shown in Figure S2a. Figure S2b displays a three-dimensional drawing of the mesh screen. Three key structure parameters are defined in a cross-sectional view of the mesh screen (see Figure S2c), in which the weft wire diameter, warp wire diameter, and superficial pore diameter are δ_{we} = 83.63 μm, δ_{wa} = 117.58 μm, and d_p = 35 μm, respectively. d_p represents the maximum diameter through which a sphere particle just passes. The coated mesh screen was characterized in aspects of micro/nanostructure (SEM), chemical composition (energy-dispersive X-ray analysis (EDS), and X-ray diffraction (XRD)), wettability, and ability of water resistance to achieve the best parameters of the fabrication process. The contact angle and sliding angle of a water droplet reveal the wettability of the mesh screen, which are measured

https://doi.org/10.1021/acs.langmuir.1c00585
Langmuir 2021, 37, 6257−6267

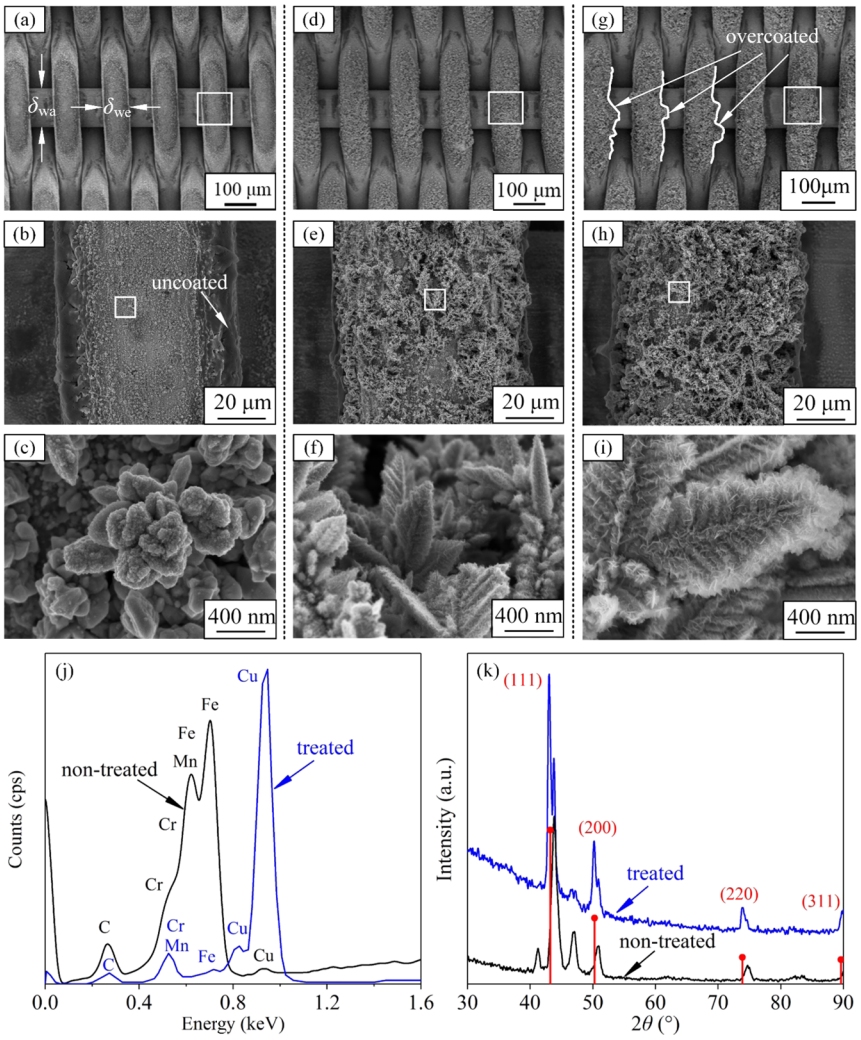

Figure 3. Characterization of the superhydrophobic/oleophilic mesh screen. (a–c, d–f, g–i) SEM images of the meshes with immersion durations of 7, 20, and 30 s, respectively. The weft wire diameter δ_{we} = 83.63 μm and the warp wire diameter δ_{wa} = 117.58 μm. (j) EDS analysis of pristine and treated meshes. (k) XRD analysis of both samples.

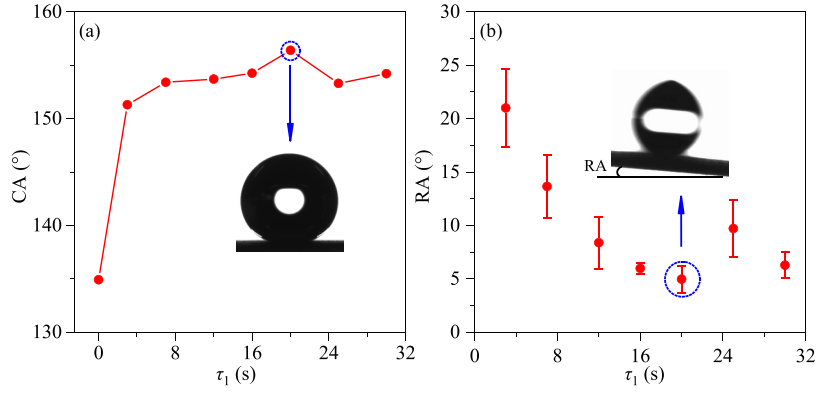

Figure 4. Contact angles (a) and sliding angles (b) of a water droplet on the mesh screen surface versus chemical treating time τ_1 in a copper sulfate solution (note: the immersion time in a stearic acid alcohol solution is 30 min).

by a contact angle measuring instrument (OCA 15EC, DATA PHYSICS, Germany) using 3.5 μL of deionized water droplets. Five different positions were measured on the sample to get mean values as the contact angle or rolling angle. Two experiments were carried out to obtain the water column height and the droplet bounce height, representing excellent properties of the mesh screen to block the water outside of the device. Furthermore, the process of oil spreading and permeating through the mesh screen could display the oil–water separation ability.

RESULTS AND DISCUSSION

Properties of the Modified Mesh Screen. Figure 3 shows the surface morphology and chemical composition of

https://doi.org/10.1021/acs.langmuir.1c00585
Langmuir 2021, 37, 6257–6267

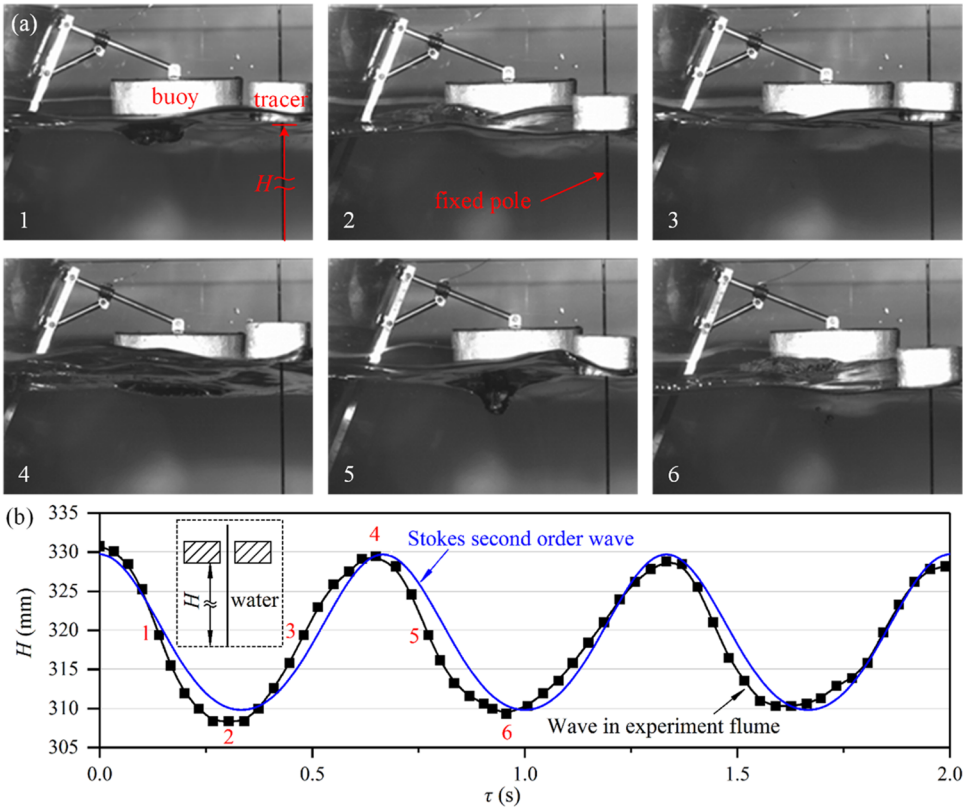

Figure 5. Wave propagation in water flume: (a) side view of a wave at six specific times and (b) comparison between the measured wave form and predictions using the Stokes wave theory.

meshes at different immersion times in the solution mixture. More microstructures on a mesh surface generate as extending immersion duration of step 1 (see Figure 3a,d,g). In the case of 7 s immersion, stone-shaped micro-/nanostructures uniformly adhere to the wire surface (see Figure 3b,c). When the immersion time was extended to 30 s, the leaf-like structures with nanoscale villus are observed to rough up the surface (see Figure 3e,f). However, the longer immersion time worsens the modification effect just like the case for immersion time of 30 s. A number of leaf structures grow sideways from the metal wire, blocking the pores of the mesh screen (see Figure 3g,h). It is noted that the leaf structures are in microscale, while the villi on leaf structures are about tens of nanometers (see Figure 3f,i). These two scale-level structures are very helpful to prepare superhydrophobic or superhydrophilic surfaces since the geometrical structure plays a key role in determining surface wettability.[2,23]

From EDS and XRD analysis of raw and coated meshes, metallic Cu is verified to be formed on the surfaces of mesh wires, generating the leaf-like structures after chemical treatment (Figure 3j,k). The formation of elementary Cu on the steel wires likely follows the chemical redox reaction Fe + Cu^{2+} = Fe^{2+} + Cu, since the blue copper sulfate solution gradually transitions to green in the preparation process.[16] This reflects that the Fe^{2+} concentration in the solution is increased as the reaction takes place.

The surface wettability was evaluated using the contact angle and the sliding angle. Figure 4 shows the variation of contact angles and sliding angles of a water droplet on the coated mesh screen for specified immersion duration (τ_1 = 0−30 s) in a $CuSO_4$ and HCl solution. The exposure time to a stearic acid solution was 30 min for all cases. It is found that both the contact angle and the sliding angle are greatly affected by immersion duration time τ_1. The rougher surface is beneficial to obtain superhydrophobicity due to the decrease in the water−solid contact area.[4] The static contact angle increases with the increase of immersion duration and then remains stable after a certain duration of ∼20 s. The rolling angle decreases when the immersion time is extended, presenting a small fluctuation after the critical duration. The optimized duration time is selected as 20 s. Moreover, the stearic acid solution offers $-CH_3$ and $-CH_2$ groups that reduce the surface energy of Cu-active components, making the mesh screen repellent to water. The modified mesh screen exhibits strong hydrophobicity, and the water contact and sliding angles approach 156.4 and 4.9°, respectively (see Figure 4a,b).

We note that the outer surface of the mesh screen is a stearic acid layer, enhancing the nanocoating strength by generating copper stearate.[24] To test how strong the modified mesh screen surface is, two additional experiments were performed. The first experiment tested the maximum static pressure of water that can be maintained by the mesh screen (see Figure S3a). In such an experiment, water was gradually dripped into a glass container whose bottom was sealed by a piece of the prepared mesh screen sample. The dripping process was stopped until the water was leaked through the mesh screen, under which the maximum static pressure was generated. The test outcome indicated a maximum static pressure of 437.3 mm water column, corresponding to a static pressure of 4.3 kPa. The second experiment tested the maximum dynamic load that can be sustained by the mesh screen. The water droplet jumping experiment was performed for such a purpose. A ∼1.88 mm diameter droplet was used. When an initial droplet height above the horizontal mesh screen plane is smaller than a

https://doi.org/10.1021/acs.langmuir.1c00585
Langmuir 2021, 37, 6257−6267

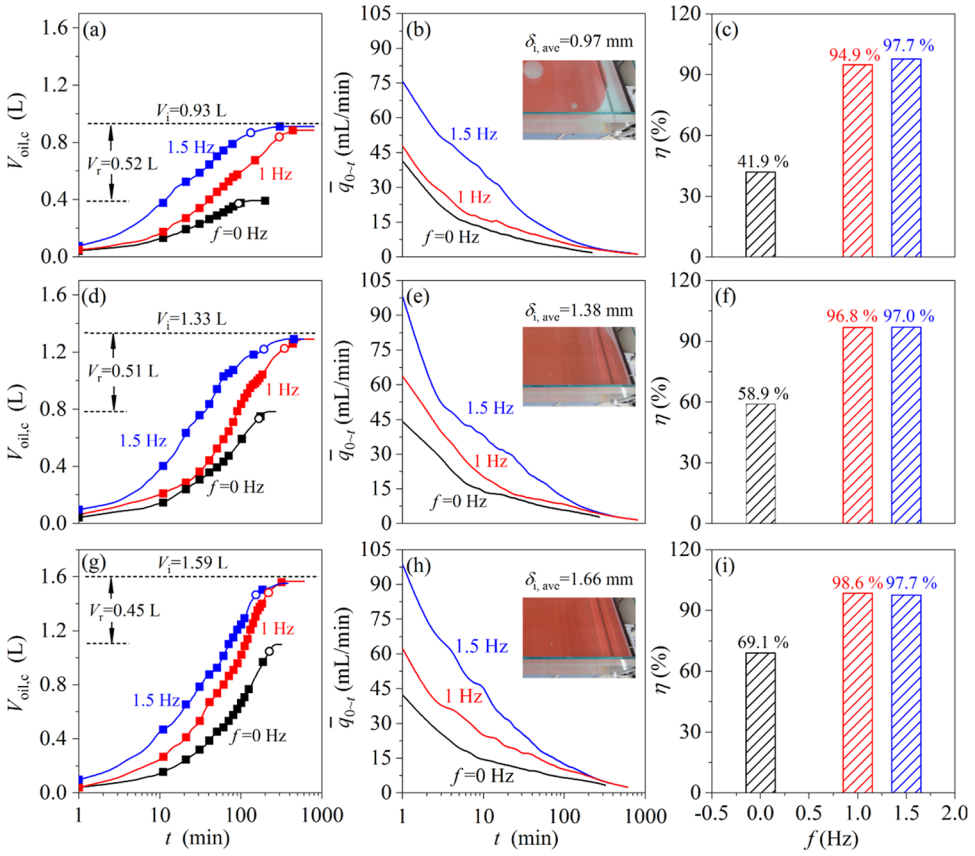

Figure 6. Oil−water separation performance with different initial oil volumes and wave frequencies: (a−c, d−f, g−i) oil−water separation performance for $\delta_{i,ave}$ of 0.97, 1.38, and 1.66 mm, respectively. The left column and middle column are collected oil versus time and average oil collection speed versus time, respectively. The right column represents oil−water separation efficiency at different wave frequencies.

critical value, droplet collision with a mesh screen yields a jumping process. However, beyond the critical height, jumping does not occur anymore, but instead, the droplet is broken up and passes through the mesh screen holes. The maximum droplet height was measured to be 17.58 cm, corresponding to an impacting velocity of 1.43 m/s (see Figure S3b). For larger impacting force, a more robust coated mesh could be applied, such as self-healing coatings,[25−27] branched fluorinated epoxy coatings,[28] and poly(dimethylsiloxane) (PDMS)-grafted-SiO_2/TiO_2@PDMS coatings.[29]

The spreading and leaking behaviors of an oil droplet over the modified mesh are studied to recognize the oleophilic properties. In the experiment, liquid paraffin was continuously dripped onto the mesh screen by a needle with a speed of 1 μL/s. The dynamic spreading and leaking behaviors of oil droplets were photographed from both the top and side views (see Figure S4). The distribution of oil droplets on the mesh wire is anisotropic due to the stress difference at the three-phase contact line.[30] With continuous oil dripping, the aggregated oil permeates through the mesh screen. A convex liquid surface is formed below the mesh screen. As the liquid gravity is greater than the surface tension force, a certain amount of oil would be separated from the convex liquid (see Figure S4b).

We note that the present experiment was performed with clean water as a working fluid. For practical applications, attention should be paid to fouling, which deteriorates oil separation and collection performance. After fouling, the device rinsing with clean water is an effective method to remove contaminants on a mesh screen separator.[31] Besides, the antifouling coatings and structures can be used to resist contaminant accumulation on the mesh screen.[32] The modified mesh screen is the key component of the separator. The fabrication of the mesh screen separator involves welding of the mesh screen with a conical stainless-steel vessel, together with chemical treatment of the mesh screen. Such a fabrication method can be scaled up and be regenerated for practical applications.

Water Wave and Oil Film Movement. The wave propagation created by a wave generator was recorded via a floating tracer and a high-speed camera (see Figure 5a). The tracer can move up and down with the wave. The high-speed camera recorded the tracer moving trails, and the wave amplitude, frequency, and wavelength can be calculated by postprocessing the captured images. Hereby, the relationship between the operation parameters of the wave generator and the key parameters of the wave is established. For example, when the stroke of the shaking tank is 8 cm and the frequency is 1.5 Hz, the amplitude, frequency, and wavelength of the induced wave are 20 ± 3 mm, 1.5 ± 0.2 Hz, and 407 ± 10 mm, respectively (see Figure 5b), which are consistent with the results predicted by the second-order equation of the Stokes wave.[33] Fitting the actual wave curve yields the following expression

$$\eta = 10\cos(0.015x - 4.187t) + 0.77\cos(0.031x - 8.374t) \quad (2)$$

https://doi.org/10.1021/acs.langmuir.1c00585
Langmuir 2021, 37, 6257−6267

It is shown that the resulting wave can be superposed from a regular sinusoidal wave.

The present study used wave energy to promote oil separation efficiency. For practical applications, the nature wave energy of river/sea can be the driving force for continuous oil separation and collection. The Froude number Fr_w makes a link between a laboratory experiment and practical applications under a sea/river environment. The Fr_w characterizes the competition between inertia force due to wave motion and gravity force of a wave above a water surface, which is written as

$$Fr_w = \frac{V_w}{\sqrt{gH_w}} \quad (3)$$

where V_w and H_w are the wave velocity and wave height, respectively. For the generator-produced wave in this experiment, V_w was 0.61 m/s and H_w was 0.02 m, yielding Fr_w = 1.38. For nature wave in sea, V_w and H_w are in the ranges of 3.31−14.5 m/s and 0.33−13.9 m, respectively,[34] corresponding to Fr_w in the range of 1.24−1.84. Hence, the present experimental results can be extended for practical applications under a sea environment based on this analogy.

In this paper, oil−water separation experiments are carried out on calm water and fluctuating water surfaces, separately. Although the oil was dyed orange-red, it was difficult to observe the spreading and flow of an oil film. To solve this problem, a tracer is placed on the oil film, and its movement is recorded by a camera (see Figure S5). On calm water, the oil flow promotes the velocity of the tracer from 0 to the same speed of oil, moving toward the separator with a speed of ∼0.47 mm/s, as displayed in Figure S5a. Close to the mesh, the tracer suddenly accelerates and attaches to the mesh (260 s), which indicates that the oil is fast sucked into the floating well and the suction speed is much faster than that of the normal oil movement. When the water surface is fluctuating, the tracer moved much faster than on calm water under the assistance of a wave, as shown in Figure S5b. In the first 7 s, the tracer travels forward 0.32 m with an average velocity of 4.57 cm/s, which is 95 times faster than that in the calm water. This reflects that wave propagation can greatly promote oil movement.

Oil−Water Separation. The oil−water separation experiment was carried out in a water flume. Three oil film thicknesses were selected. Initially, a characteristic oil film thickness δ_m was experimentally determined. By gradually oil dripping on a water surface, δ_m is defined as a value at which the whole water surface is covered by an oil layer without exposing any water dot. Here, δ_m = 1.38 mm. Then, a smaller value and a larger value were selected as $0.7\delta_m$ = 0.97 mm and $1.2\delta_m$ = 1.66 mm, respectively (see inset images in Figure 6b,e,h).

The key experimental parameters are listed in Table 1. The device floats on the water interface with mesh contacting the oil film. The inner wall of the barrel is measurably marked to quantify the oil storage per minute until the volume of collected oil V_c is unchanged anymore. At this moment, the separation efficiency of the device is calculated as $\eta = \frac{V_c}{V_i} \times 100\%$, where V_i denotes the oil mass in the water flume at the initial time. The duration for collecting $0.95V_c$ is defined as the separation time and thus the mean collection rate can be evaluated as $\overline{q}_{0-t} = \frac{V_{c,0-t}}{t}$ (see the hollow dot in Figure 6a,d,g). From data shown in Figure 6, it is obvious that the wave-driven oil collection rate is faster than that of calm water, and the separation efficiency is much higher, approaching to 99% with only 0.03 L of oil left on the water surface (see Figure 6i). These results verify the effectiveness of the floating well to separate oil in water. The oil−water separation rate increases with an increase in the wave frequency from 0 to 1.5 Hz, and the maximum collection rate is more than 2 times faster than that of calm water. However, the final wave-driven collection efficiency is insensitive to the wave frequency (Figure 6c,f,i). On calm water, the collection efficiency is only 42−69% much lower than the wave-driven cases. The left oil on the water surface is about 0.5 L, regardless of the initial thickness of the oil film, which is an insurmountable limit for oil−water separation on calm water. High-speed centrifugation was introduced to examine the purity of collected oil. As displayed in Figure S6, no free water at the bottom of the centrifugal tube was observed, indicating a high filtrate oil purity above 98 wt % or better.

To test the floating-well durability for oil separation and collection, experiments lasted for 1 month, during which 40 runs were tested. The repeated experiments were performed to test such durability (see Figure 7). For the run with an initial oil film thickness of 1.38 mm and the wave frequency of 1.0 Hz, the performance was almost identical for the 1st day measurement and the measurement performed at the end of

Table 1. Key Parameters of the Simulated Wave[a]

case no.	V_i (L)	$\delta_{i,ave}$ (mm)	frequency of shock (Hz)	A_w (mm)
1	0.93	0.97	0	0
2	0.93	0.97	1	13
3	0.93	0.97	1.5	20
4	1.33	1.38	0	0
5	1.33	1.38	1	13
6	1.33	1.38	1.5	20
7	1.59	1.66	0	0
8	1.59	1.66	1	13
9	1.59	1.66	1.5	20

[a]Note: $\delta_{i,ave}$ is the initial average thickness of the oil film and A_w is the amplitude of the water wave.

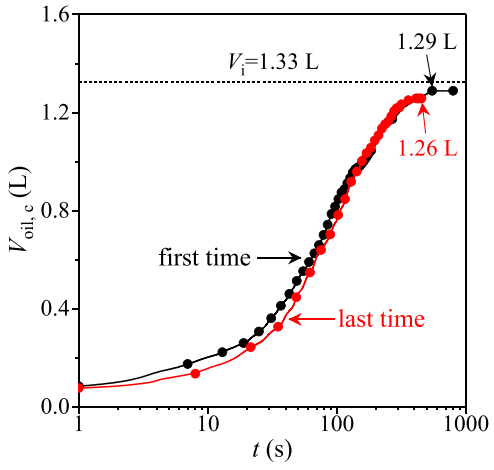

Figure 7. Collected oil volumes versus time for the 1st day measurement and the measurement performed at the end of the month.

https://doi.org/10.1021/acs.langmuir.1c00585
Langmuir 2021, 37, 6257−6267

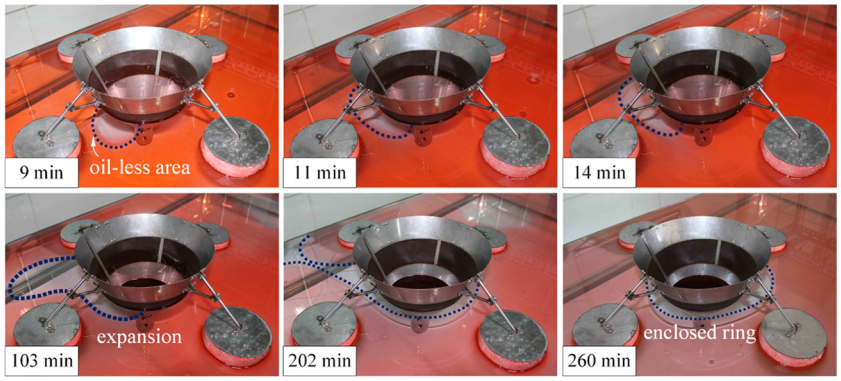

Figure 8. Formation of a water ring around the mesh screen separator on a calm water surface (note: the initial oil film thickness is 1.38 mm).

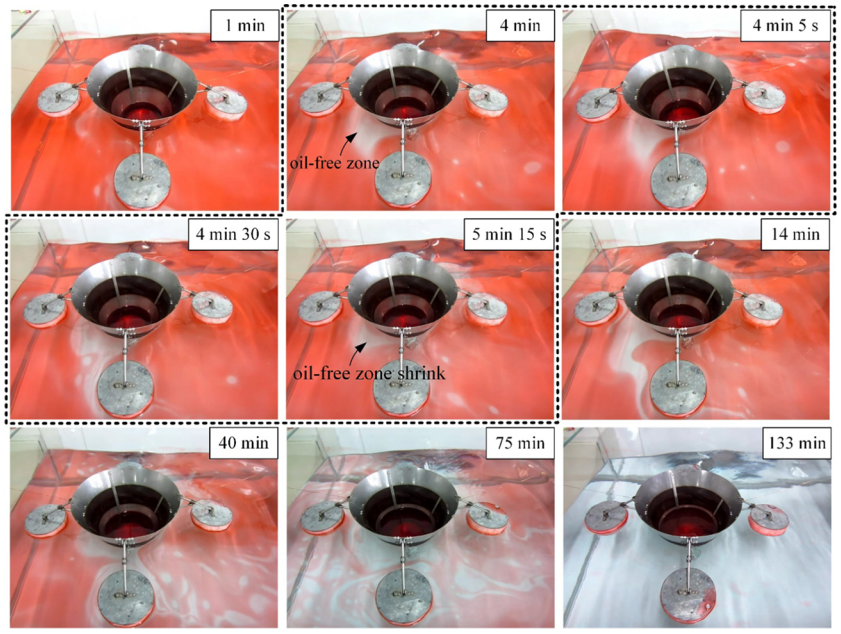

Figure 9. Oil–water separation process with the help of a water wave at 1.5 Hz frequency (note: the initial oil film thickness is 1.66 mm, corresponding to case 9 in Table 1).

the month. The final collected oil was 1.26 L, approaching the total floating oil of 1.29 L. The repeatable tests indicate that the system can sustain long-term operation at least for 1 month.

The low oil–water separation efficiency on calm water is induced by the surface tension that hinders the oil film from spreading when oil film thickness is less than a certain value, leading to oil film breakup and an oil-free zone formed around the mesh screen. Figure 8 shows the water ring formation enclosing the mesh screen. At first, the oil-free zone is only formed locally, where the oil film stops spreading. The surrounding oil film continually flows into the floating well to extend the oil-free zone until a water ring is formed around the mesh screen. This water ring prevents direct contact between the separator and the oil, and oil–water separation process stops. However, on the undulating water, the oil–water separation continuously processed (see Figure 9). The wave-driven oil travels toward the floating well to penetrate the hydrophobic/oleophilic mesh screen. Besides, the wave turbulence may clean up the oil-free zone from the floating well, keeping oil contact with the separator. In such a case, the separation process can run continuously until all of the spilled oil is completely collected, e.g., without oil detection at the water surface (133 min). Here, a question may arise that how to accelerate the separation process? A term called oil separation rate per unit wetting perimeter is defined as the scaling parameter: $Q_c = V_{oil,c}/(t \cdot L_c)$, where $V_{oil,c}$ is the oil volume to be collected, t is the separation time, and L_c is the wetting perimeter between the circular mesh screen and the oil. For the same oil to be separated, a larger L_c value reduces the separation time.

On the calm water surface, the gravity, viscous force, surface tension, and inertia force play critical roles in oil film spreading.[35,36] A group of dimensionless numbers characterize the relative importance of the mentioned forces:$Ga = \frac{gL^3}{\nu^2}$, $Bo = \frac{\Delta\rho g L^2}{|\sigma_s|}$,and $Fr = \frac{u}{\sqrt{gL}}$, where Ga is the ratio of gravity to viscous force, Bo is the ratio of gravity to surface tension, and Fr is the ratio of inertial force to gravity. Here, g is the gravity acceleration (m/s^2), L is the thickness of the oil film (m), ν is the kinetic viscosity (m^2/s) of liquid paraffin, which is 25.29 × 10^{-6} m^2/s, $\Delta\rho$ is the density difference of oil and water (kg/m^3), σ_s is the absolute value of the spreading coefficient (N/m), defined as $\sigma_s = \gamma_o - \gamma_w - \gamma_{o-w}$ in which γ_o, γ_w, and γ_{o-w} are

https://doi.org/10.1021/acs.langmuir.1c00585
Langmuir 2021, 37, 6257–6267

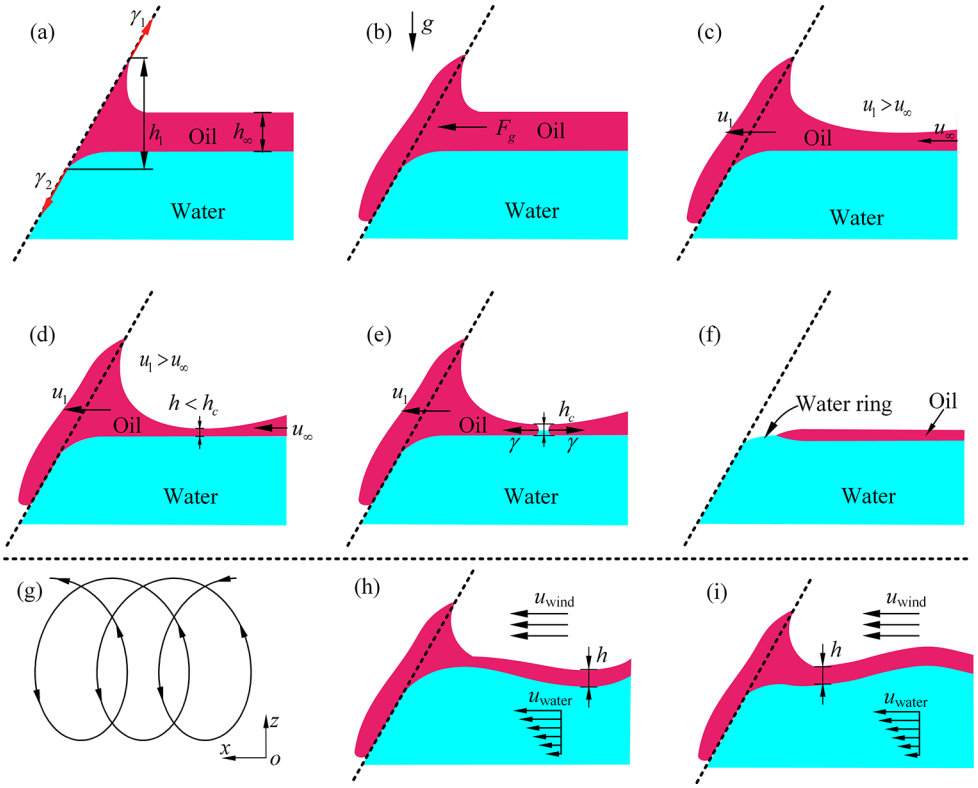

Figure 10. Mechanism of water ring formation (a–f) and wave-driven oil recovery (g–i).

surface tension of oil, water, and interfacial tension between water and oil, respectively, and u is the traveling velocity of the oil film (m/s). In our experiments, *Ga*, *Bo*, and *Fr* are in the ranges of $14-70 \times 10^{-3}$, $6.9-20.3 \times 10^{-3}$, and $3.7-4.8 \times 10^{-3}$, highlighting the dominant role of gravity in the movement of the oil film. The maximum spreading area is achieved when the gravity force is balanced by surface tension, and the critical thickness of the oil film is calculated as[36]

$$h_c = \sqrt{\frac{-2\sigma_s \rho_w}{g\rho_o(\rho_w - \rho_o)}} \tag{4}$$

where ρ_o and ρ_w are the densities of oil and water. No matter what the initial oil volume is, the critical thickness is constant. At ambient temperature, γ_w, γ_o, and γ_{o-w} are 0.0725, 0.0289, and 0.0437 N/m, respectively. As a result, the spreading coefficient σ_s is about -1×10^{-4} N/m. The critical thickness of liquid paraffin is ~0.4 mm, agreeing with the measured value of ~0.34 mm. Hence, it is the surface tension that prevents the oil film from spreading when a water ring forms.

Combining with the analysis above, one can get the oil flow process during the oil–water separation. At the initial time, the oil film thickness h_∞ is larger than the critical thickness h_c. The gravity drives the oil film to spread, and the coated mesh screen is in contact with the oil. Dominated by surface tension, the oil film thickness attached to the coated mesh screen (h_1) is similar at different thicknesses and larger than that at infinity (h_∞). Thus, the initial collection rates are similar in different cases on calm water (see Figure 6b,e,h). Due to the interaction between gravity and the mesh screen, oil–water separation occurs (see Figure 10a,b). However, the supplement oil flow from infinity to the floating well depends on the gravity-dominated spreading. The infiltration velocity u_1 of the oil film at the coated mesh screen is large than the film velocity u_∞ at infinity (see Figure 10c), which is verified in Figure S5a. With the decrease in the oil film thickness, the surface tension and viscous force gradually dominate the spreading due to the weak gravity effect (see Figure 10d). Under such circumstances, the oil film breaks up near the floating well to form the oil-free zone to terminate the oil–water separation (see Figure 10e). The gravity force is balanced by surface tension, and the water ring stably exists (see Figure 10f) and the oil film cannot spread anymore at 260 min (see Figure 8).

In contrast, the separation rate and efficiency are significantly improved with the help of the wave. The movement of oil film follows the wave propagation due to the momentum exchange between oil and water. The Stokes wave theory tells us that the displacement of fluid particles is small along the wave propagation direction (see Figure 10g), indicating that mass migration exists at the water surface.[33] The net displacement of the water surface in a period is

$$\Delta x = \frac{1}{2}\pi^2\left(\frac{A_w}{L_w}\right)^2 \frac{\omega}{k}\frac{\cosh 2kH}{\sinh^2 kH}T \tag{5}$$

where A_w, L_w, ω, k, and T are the wave amplitude, wavelength, angular frequency, wavenumber, and period, respectively. Based on eq 2, for the wave frequency of 1.5 Hz, the net displacement is 9.7 mm and the average traveling speed is 14.6 mm/s. Alternatively, for the 1.0 Hz frequency, the net displacement and the traveling speed are 8.9 mm and 8.9 mm/s, respectively. Therefore, the separation rate at 1.5 Hz is larger than that of 1.0 Hz due to the faster oil transportation. The wave propels the oil moving toward the floating well and prevents the formation of the water ring. The oil–water separation rate and efficiency are much larger on a waved water surface than those on a calm water surface. In practice, the air–

https://doi.org/10.1021/acs.langmuir.1c00585
Langmuir 2021, 37, 6257–6267

water flow helps to propel the oil moving toward the floating well (see Figure 10h,i).

The present experiment was performed using clean water and oil. For practical applications, the effect of salt concentration on oil separation should be considered. The surface tension of salt water was measured by Shah et al.[37] They noted that surface tension and the contact angle of water increased with an increase in salt concentrations, indicating the increased superhydrophobic degree of a mesh screen with respect to water when salt concentration increases. This effect prevents direct contact between the mesh screen and water, which is a positive effect for oil separation. In summary, our work presents a new clue for large-scale in situ applications, in which the nature wave energy of river/sea can be the driving force for continuous oil separation and collection.

CONCLUSIONS

An in situ oil−water separating system, called a floating well, is invented for large-scale applications, including a modified mesh screen for water−oil separation and a container for oil storage. To verify the effectiveness of the system, the oil removal experiment was performed both on calm water and waved water in a glass container. The floating well is shown to have excellent stability for all tests. On the calm water surface, due to the breakdown of the thin oil film, oil-free areas were observed to encircle the floating well, preventing the direct contact between the separator and the oil. Thus, the measured oil collection efficiency is only 42−69%. In contrast, with the low-frequency surface wave, the oil collection efficiency increased sharply to 98%, under which the collection speed was 2.5 times that on the calm water surface. The wave continuously drives the oil film toward the separator from elsewhere, and almost all of the spilled oil was completely collected. This work presents an important strategy to design and operate large-scale wave-driven in situ oil separation system, in which the nature wave energy of river/sea can be the driving force for continuous oil separation and collection.

ASSOCIATED CONTENT

Supporting Information

The Supporting Information is available free of charge at https://pubs.acs.org/doi/10.1021/acs.langmuir.1c00585.

> Key parameters of liquid paraffin, fabrication of the superhydrophobic/oleophilic mesh screen, images of the twill Dutch weaved mesh screen, water resistance of the superhydrophobic/oleophilic mesh screen, oil spreading on the mesh screen, visualization of oil film movement, and the collected oil without apparent water droplets after centrifugation (PDF)

AUTHOR INFORMATION

Corresponding Author

Xiaojing Ma − *Beijing Key Laboratory of Multiphase Flow and Heat Transfer for Low Grade Energy Utilization, North China Electric Power University, Beijing 102206, China; Key Laboratory of Power Station Energy Transfer Conversion and System, Ministry of Education, North China Electric Power University, Beijing 102206, China;* orcid.org/0000-0003-3246-3942; Email: mxj@ncepu.edu.cn

Authors

Xin Yan − *Beijing Key Laboratory of Multiphase Flow and Heat Transfer for Low Grade Energy Utilization, North China Electric Power University, Beijing 102206, China; National Institute of Clean-and-Low-Carbon Energy (NICE), Beijing 102211, China*

Guohua Liu − *Beijing Key Laboratory of Multiphase Flow and Heat Transfer for Low Grade Energy Utilization, North China Electric Power University, Beijing 102206, China; Key Laboratory of Power Station Energy Transfer Conversion and System, Ministry of Education, North China Electric Power University, Beijing 102206, China;* orcid.org/0000-0003-3401-1851

Jinliang Xu − *Beijing Key Laboratory of Multiphase Flow and Heat Transfer for Low Grade Energy Utilization, North China Electric Power University, Beijing 102206, China; Key Laboratory of Power Station Energy Transfer Conversion and System, Ministry of Education, North China Electric Power University, Beijing 102206, China;* orcid.org/0000-0003-0145-9983

Complete contact information is available at: https://pubs.acs.org/10.1021/acs.langmuir.1c00585

Notes

The authors declare no competing financial interest.

ACKNOWLEDGMENTS

The authors acknowledge the support from the Nature Science Foundation of China (52076077 and 51821004) and the Fundamental Research Funds for the Central Universities (2020DF002).

REFERENCES

(1) Jernelöv, A. How to defend against future oil spills. *Nature* **2010**, *466*, 182−183.

(2) Wang, B.; Liang, W.; Guo, Z.; Liu, W. Biomimetic super-lyophobic and super-lyophilic materials applied for oil/water separation: a new strategy beyond nature. *Chem. Soc. Rev.* **2015**, *44*, 336−361.

(3) Gupta, R. K.; Dunderdale, G. J.; England, M. W.; Hozumi, A. Oil/water separation techniques: a review of recent progresses and future directions. *J. Mater. Chem. A* **2017**, *5*, 16025−16058.

(4) Ge, J.; Zhao, H. Y.; Zhu, H. W.; Huang, J.; Shi, L. A.; Yu, S. H. Advanced Sorbents for Oil-Spill Cleanup: Recent Advances and Future Perspectives. *Adv. Mater.* **2016**, *28*, 10459−10490.

(5) Hoang, A. T.; Chau, M. Q. A Mini Review of Using Oleophilic Skimmers for Oil Spill Recovery. *J. Mech. Eng. Res. Dev.* **2018**, *41*, 92−96.

(6) Ge, J.; Shi, L. A.; Wang, Y. C.; Zhao, H. Y.; Yao, H. B.; Zhu, Y. B.; Zhang, Y.; Zhu, H. W.; Wu, H. A.; Yu, S. H. Joule-heated graphene-wrapped sponge enables fast clean-up of viscous crude-oil spill. *Nat. Nanotechnol.* **2017**, *12*, 434−440.

(7) Zhu, Z.; Wang, W.; Qi, D.; Luo, Y.; Liu, Y.; Xu, Y.; Cui, F.; Wang, C.; Chen, X. Calcinable Polymer Membrane with Revivability for Efficient Oily-Water Remediation. *Adv. Mater.* **2018**, *30*, No. 1801870.

(8) Xue, C.-H.; Li, Y.-R.; Hou, J.-L.; Zhang, L.; Ma, J.-Z.; Jia, S.-T. Self-roughened superhydrophobic coatings for continuous oil−water separation. *J. Mater. Chem. A* **2015**, *3*, 10248−10253.

(9) Saleem, J.; Adil Riaz, M.; Gordon, M. Oil sorbents from plastic wastes and polymers: A review. *J. Hazard. Mater.* **2018**, *341*, 424−437.

(10) Li, J.; Li, D.; Yang, Y.; Li, J.; Zha, F.; Lei, Z. A prewetting induced underwater superoleophobic or underoil (super) hydro-

phobic waste potato residue-coated mesh for selective efficient oil/water separation. *Green Chem.* **2016**, *18*, 541−549.
(11) Feng, S.; Xing, Y.; Deng, S.; Shang, W.; Li, D.; Zhang, M.; Hou, Y.; Zheng, Y. An Integrative Mesh with Dual Wettable On-Off Switch of Water/Oil. *Adv. Mater. Interfaces* **2018**, *5*, No. 1701193.
(12) Kong, W. T.; Pan, Y. L.; Bhushan, B.; Zhao, X. Z. Superhydrophilic Al2O3 Particle Layer for Efficient Separation of Oil-in-Water (O/W) and Water-in-Oil (W/O) Emulsions. *Langmuir* **2020**, *36*, 13285−13291.
(13) Wang, B. Y.; Ma, Y. L.; Ge, H. Q.; Luo, J.; Peng, B.; Deng, Z. W. Design and Synthesis of Self-Healable Superhydrophobic Coatings for Oil/Water Separation. *Langmuir* **2020**, *36*, 15309−15318.
(14) Liu, Y. Q.; Jiao, Z. Z.; Zhang, Y. L.; Liu, Y.; Jiang, H. B.; Han, D. D.; Sun, H. B. Kraft Mesh Origami for Efficient Oil-Water Separation. *Langmuir* **2019**, *35*, 815−823.
(15) Zhang, S.; Jiang, G.; Gao, S.; Jin, H.; Zhu, Y.; Zhang, F.; Jin, J. Cupric Phosphate Nanosheets-Wrapped Inorganic Membranes with Superhydrophilic and Outstanding Anticrude Oil-Fouling Property for Oil/Water Separation. *ACS Nano* **2018**, *12*, 795−803.
(16) Song, J.; Lu, Y.; Luo, J.; Huang, S.; Wang, L.; Xu, W.; Parkin, I. P. Barrel-Shaped Oil Skimmer Designed for Collection of Oil from Spills. *Adv. Mater. Interfaces* **2015**, *2*, No. 1500350.
(17) Chen, N.; Pan, Q. Versatile fabrication of ultralight magnetic foams and application for oil-water separation. *ACS Nano* **2013**, *7*, 6875−6883.
(18) Zhu, Q.; Tao, F.; Pan, Q. Fast and selective removal of oils from water surface via highly hydrophobic core-shell Fe_2O_3@C nanoparticles under magnetic field. *ACS Appl. Mater. Interfaces* **2010**, *2*, 3141−3146.
(19) Chang, J.; Shi, Y.; Wu, M.; Li, R.; Shi, L.; Jin, Y.; Qing, W.; Tang, C.; Wang, P. Solar-assisted fast cleanup of heavy oil spills using a photothermal sponge. *J. Mater. Chem. A* **2018**, *6*, 9192−9199.
(20) Ou, R.; Wei, J.; Jiang, L.; Simon, G. P.; Wang, H. Robust Thermoresponsive Polymer Composite Membrane with Switchable Superhydrophilicity and Superhydrophobicity for Efficient Oil-Water Separation. *Environ. Sci. Technol.* **2016**, *50*, 906−914.
(21) Bazyar, H.; van de Beek, N.; Lammertink, R. G. H. Liquid-Infused Membranes with Oil-in-Water Emulsions. *Langmuir* **2019**, *35*, 9513−9520.
(22) Oh, S.; Ki, S.; Ryu, S.; Shin, M. C.; Lee, J.; Lee, C.; Nam, Y. Performance Analysis of Gravity-Driven Oil-Water Separation Using Membranes with Special Wettability. *Langmuir* **2019**, *35*, 7769−7782.
(23) Cherukupally, P.; Sun, W.; Wong, A. P. Y.; Williams, D. R.; Ozin, G. A.; Bilton, A. M.; Park, C. B. Surface-engineered sponges for recovery of crude oil microdroplets from wastewater. *Nat. Sustainability* **2020**, *3*, 136−143.
(24) Xu, N.; Sarkar, D. K.; Grant Chen, X.; Zhang, H.; Tong, W. Superhydrophobic copper stearate/copper oxide thin films by a simple one-step electrochemical process and their corrosion resistance properties. *RSC Adv.* **2016**, *6*, 35466−35478.
(25) Rao, Q.; Chen, K.; Wang, C. Facile preparation of self-healing waterborne superhydrophobic coatings based on fluoroalkyl silane-loaded microcapsules. *RSC Adv.* **2016**, *6*, 53949−53954.
(26) Zhu, D.; Lu, X.; Lu, Q. Electrically Conductive PEDOT Coating with Self-Healing Superhydrophobicity. *Langmuir* **2014**, *30*, 4671−4677.
(27) Hönes, R.; Ruehe, J. Extending the Lotus Effect: Repairing Superhydrophobic Surfaces after Contamination or Damage by CHic Chemistry. *Langmuir* **2018**, *34*, 8661−8669.
(28) Zhu, K.; Zhang, J.; Zhang, H.; Tan, H.; Zhang, W.; Liu, Y.; Zhang, H.; Zhang, Q. Fabrication of durable superhydrophobic coatings based on a novel branched fluorinated epoxy. *Chem. Eng. J.* **2018**, *351*, 569−578.
(29) Peng, S.; Meng, W.; Guo, J.; Wang, B.; Wang, Z.; Xu, N.; Li, X.; Wang, J.; Xu, J. Photocatalytically Stable Superhydrophobic and Translucent Coatings Generated from PDMS-Grafted-SiO2/TiO2@PDMS with Multiple Applications. *Langmuir* **2019**, *35*, 2760−2771.
(30) Xie, J.; Xu, J.; Liang, C.; She, Q.; Li, M. A comprehensive understanding of enhanced condensation heat transfer using phase separation concept. *Energy* **2019**, *172*, 661−674.
(31) Tijing, L. D.; Woo, Y. C.; Choi, J.-S.; Lee, S.; Kim, S.-H.; Shon, H. K. Fouling and its control in membrane distillation—A review. *J. Membr. Sci.* **2015**, *475*, 215−244.
(32) Liu, G.; Chen, T.; Xu, J.; Yao, G.; Xie, J.; Cheng, Y.; Miao, Z.; Wang, K. Salt-Rejecting Solar Interfacial Evaporation. *Cell Rep. Phys. Sci.* **2021**, *2*, No. 100310.
(33) Sundar, V. *Ocean Wave Mechanics: Applications in Marine Structures*; John Wiley & Sons, 2017; p 280.
(34) Thurman, H. V.; Trujillo, A. P. *Introductory Oceanography*, 10th ed.; Prentice Hall, Inc.: Upper Saddle River, NJ, 2004.
(35) Hoult, D. P. Oil Spreading on the Sea. *Annu. Rev. Fluid Mech.* **1972**, *4*, 341−368.
(36) Nikolov, A.; Wasan, D. Oil lenses on the air-water surface and the validity of Neumann's rule. *Adv. Colloid Interface Sci.* **2017**, *244*, 174−183.
(37) Shah, A.-u.-H. A.; Ali, K.; Bilal, S. Surface tension, surface excess concentration, enthalpy and entropy of surface formation of aqueous salt solutions. *Colloids Surf., A* **2013**, *417*, 183−190.

https://doi.org/10.1021/acs.langmuir.1c00585
Langmuir 2021, 37, 6257−6267